Title:

Polymorphism within a neuronal activity-dependent enhancer of *NgR1* is associated with corpus callosum morphology in humans

Short title for use as running head:

NgR1 is associated with corpus callosum morphology

Masanori Isobe[1] MD, Kenji Tanigaki[2,*] MD, PhD, Kazue Muraki[2] BSc, Jun Miyata[1] MD, PhD, Ariyoshi Takemura[1] MD, Genichi Sugihara[1] MD, PhD, Hidehiko Takahashi[1] MD, PhD, Toshihiko Aso[3] MD, PhD, Hidenao Fukuyama[3] MD, PhD, Masaaki Hazama[1] MD, PhD, and Toshiya Murai [1,*] MD, PhD

Author Affiliation:

Department of Psychiatry, Graduate School of Medicine, Kyoto University, Japan

*Corresponding authors

Toshiya Murai, MD, PhD

Department of Psychiatry, Graduate School of Medicine, Kyoto University

54 Shogoin-Kawahara-cho, Sakyo-ku, Kyoto 606-8507, Japan

E-mail: murai@kuhp.kyoto-u.ac.jp; Tel: +81-75-751-3386; Fax: +81-75-751-3246

Kenji Tanigaki, MD, PhD

Research Institute, Shiga Medical Center

5-4-30 Moriyama, Moriyama, Shiga 524-8524, Japan

E-mail: tanigaki@res.med.shiga-pref.jp; Tel: +81-77-582-6048; Fax: +81-77-582-6041

Keywords:

Nogo-66 receptor 1, corpus callosum, magnetic resonance imaging, diffusion tensor imaging, genetic polymorphism, bioinformatics, epigenomics, luciferase assay, electrophoretic mobility shift assay

Abstract

The human Nogo-66 receptor 1 (*NgR1*) gene, also termed as the Nogo receptor 1 or Reticulon 4 receptor (*RTN4R*) and located within 22q11.2, inhibits axonal growth and synaptic plasticity. 22q11.2 deletion syndrome (22q11.2DS) patients show multiple changes in brain morphology, with corpus callosum (CC) abnormalities being among the most prominent and frequently reported. Thus, we hypothesized that in humans, *NgR1* may be involved in CC formation. We focused on rs701428, a single nucleotide polymorphism of *NgR1*, which is associated with schizophrenia. We investigated the effects of rs701428 genotype on CC structure in 50 healthy participants using magnetic resonance imaging (MRI). Polymorphism of rs701428 was associated with CC structural variation in healthy participants; specifically, minor A allele carriers had larger whole CC volumes and lower radial diffusivity in the central CC region compared with major G allele homozygous participants. Furthermore, we show that the *NgR1* 3' region, which contains rs701428, is a neuronal activity-dependent enhancer, and that the minor A allele of rs701428 is susceptible to regulation of enhancer activity by MYBL2. Our results suggest that *NgR1* can influence macro- and micro- white matter structure of the human brain. (188 words)

Introduction

In humans, the Nogo-66 receptor 1 (*NgR1*) gene, which gene is also termed as the Nogo receptor 1 or Reticulon 4 receptor (*RTN4R*), is located within the 22q11.2 locus. NgR1 can bind (1) Nogo-A, (2) myelin associated glycoprotein, and (3) oligodendrocyte myelin glycoprotein. These proteins are myelin-associated inhibitors of axonal regeneration [1-4]. Previous research has shown that *NgR1* plays a role in the inhibition of axonal growth and synaptic plasticity [5, 6]. *NgR1* is widely expressed in the central nervous system [7], including in neurons of the neocortex, hippocampus, amygdala, and dorsal thalamus [8].

22q11.2 deletion syndrome (22q11.2DS) is caused by a genomic microdeletion within chromosomal region 22q11.2, which contains as many as 35–60 genes [9]. Patients with this syndrome develop schizophrenia at a substantially increased rate of 25–30%, which is approximately 25–31 times higher than the general population [10]. Thus, this deletion has drawn attention as a potential model to determine the key pathophysiology of schizophrenia [11, 12].

The deletion is associated with various types of structural brain alterations: cavum septum pellucidum, cavum vergue [13, 14], polymicrogyria [15], enlarged ventricles [13, 16], decreased volume of total brain [14, 16], cerebellum [13] and hippocampus [17], volume change of specific subcortical structures, including corpus callosum [18-20], reduced fractional anisotropy (FA) in areas of the frontal, parietal and temporal lobes [21, 22], and increased FA from the posterior corpus callosum (CC) to the occipital lobes [22]. Of these alterations, abnormalities in the CC [18-20], the largest interhemispheric tract connecting the association cortices, are among the most prominent and consistently reported in 22q11.2DS. Some of these structural anomalies,

including enlarged corpus callosum, are also observed in sporadic schizophrenia [20, 23-25].

Here we focused on rs701428, an *NgR1* single nucleotide polymorphism (SNP) that shows association with schizophrenia in Caucasian and African-American populations [26, 27]. Association between allelic variation of this SNP and diffusion tensor imaging (DTI) metrics of the white matter tract has been reported in 22q11.2 DS patients [28]. To examine the roles of *NgR1* in the CC formation, we investigated possible association between *NgR1* genetic variation and CC structure in healthy participants, using structural magnetic resonance imaging (MRI) and DTI. We also examined the physiological function of rs701428 by combining *in silico* and *in vitro* approaches.

Materials and Methods

Participants

Fifty healthy individuals were recruited from the local community. None had a history of psychiatric disease, as determined by the non-patient edition of the Structured Clinical Interview for DSM-IV Axis I Disorders (SCID). In addition, none had a history of head trauma, neurological disease, severe medical diseases, or substance abuse. There was no history of psychotic disorders among first-degree relatives. Participants were all physically healthy at the time of scanning. This study was approved by the Committee on Medical Ethics of Kyoto University and was performed according to The Code of Ethics of the World Medical Association. Written informed consent was obtained from each participant.

NgR1 genotyping

Genomic DNA was extracted from venous blood samples of each participant using standard methods, with ethylene-diaminetetraacetic acid anticoagulant. The SNP rs701428 was genotyped using the LightCycler 480 system (Roche, Basel, Switzerland) and a TaqMan SNP Genotyping Assay (TaqMan SNP Genotyping Assay ID C_2785952_10; Applied Biosystems, Foster City, CA, USA).

MRI acquisition

All participants were scanned with a 3 T MRI scanner (Trio; Siemens, Erlangen, Germany). Diffusion-weighted imaging data were acquired using single-shot spin-echo echo-planar sequences. Structural MRI data were obtained using three dimensional magnetization-prepared rapid gradient echo (3 D-MPRAGE) sequences, with a 40 mT/m gradient and a receiver-only eight-channel phased-array head coil. The parameters for diffusion-weighted data were: echo time (TE) 96 ms; repetition time (TR) 10 500 ms; 96 × 96 matrix; field of view (FOV) 192 × 192 mm; 70 contiguous axial slices of 2.0 mm thickness; 81 non-co-linear axis motion-probing gradients; and b = 1 500 s/mm^2. The b = 0 images were scanned before every nine diffusion-weighted images, hence 90 volumes in total. The parameters for 3 D-MPRAGE imaging data were: TE 4.38 ms; TR 2000 ms; inversion time 990 ms; 240 × 256 matrix; FOV 225 × 240 mm; resolution, 0.9375 × 0.9375 × 1.0 mm^3; and 208 total axial sections without intersection gaps.

Imaging data preprocessing

DTI data preprocessing

All DTI data processing was performed using programs in the Functional MRI of the

Brain (FMRIB) Software Library (FSL) version 4.1.6 (http://www.fmrib.ox.ac.uk/fsl). Source data were corrected for head motion and eddy currents by registering all data to the first b = 0 image with affine transformation. Fractional anisotropy (FA) maps and indices of white matter integrity were calculated using the DTIFIT program of FSL. In addition, axial diffusivity (AD) and radial diffusivity (RD), measures of diffusivity parallel and perpendicular to axons, respectively, were calculated. TBSS version 1.2 in FSL was used to normalize all FA data into the MNI 152 space. FMRIB's Nonlinear Image Registration Tool (FNIRT) was used for nonlinear transformation. Normalized FA images were averaged and thinned to create a mean skeletonized FA image, taking only centers of white matter tracts common to all subjects. Voxel values of each subject's normalized FA map were projected onto the FA skeleton by searching for the local maxima along the perpendicular direction from the skeleton. Resultant skeletonized FA data were used in the following statistical analysis. The same transformations were applied to AD and RD images to create skeletonized AD and RD maps.

Structural MRI data preprocessing

The three-dimensional magnetization-prepared rapid gradient-echo imaging (3D MPRAGE) images were preprocessed using the FreeSurfer software package version 5.0.0 (http://surfer.nmr.mgh.harvard.edu). The process included Talairach transformation of each subject's native brain, removal of non-brain tissue, volumetric subcortical labeling, and surface-based segmentation of gray and white matter tissue. In automatic segmentation, each voxel in normalized brain volumes was assigned a label based on an atlas containing probabilistic information about structure locations, including the CC. Subdivided cerebral white matter regions were derived from cortical

parcellation.

Regions of interest (ROI) setting using FreeSurfer

To define CC regions of interest (ROI), we used automatic segmentation in FreeSurfer [29], based on subcortical parcellation, which segments the CC into anterior, middle anterior, central, middle posterior, and posterior regions. Volumes of each region were automatically calculated during the segmentation process. “Whole CC” was the sum of the five subregions. Masks derived from these ROI were used to measure DTI indices (FA, AD, and RD) of the whole and segmented CC. To determine DTI indices of the CC in the diffusion space, ROI derived from FreeSurfer template images were transformed from a MNI 302 space to a MNI 152 space by applying the rigid-body transformation matrix, which was calculated using FSL’s FLIRT program. To check transformation quality and to confirm there were no gross transformation errors, we overlaid each CC ROI onto the FMRIB58_FA image, a mean FA template in the MNI 152 space, (Figure 1).

Data analysis

Group comparison of demographic data

Minor A allele carriers are associated with schizophrenia [26] and, therefore, we compared the minor A carrier group (A carrier group) with the homozygote wild-type G carrier group (G homozygous group). Demographic data and ROI volumes were analyzed by two-sample *t*-tests using SPSS 19.0 (SPSS Inc., Chicago, IL, USA.). Statistical significance was defined as $P < 0.05$ (two tailed) in all analyses.

Group comparison of volume and DTI indices of whole CC

To investigate differences in whole CC volumes between G homozygous and A carrier

groups, we adjusted the volume by the intracranial volume of each patient [30]. The white matter volume of the whole brain was also measured. In addition, we calculated mean FA, AD, and RD in the whole CC mask by multiplying CC mask and skeletonized maps. We determined significant differences using unpaired two sample *t*-tests, with the statistical threshold defined as $P < 0.05$ (two tailed).

Group comparison of volume and diffusivity in CC ROI

Next, when we detected a group difference in CC total volume, we investigated volume differences in CC ROI between G homozygous and A carrier groups to determine which CC subregion was most responsible for the volume differences observed. We determined significant differences using unpaired two sample *t*-tests, with the statistical threshold at $P < 0.01$ (= 0.05/5). We also calculated mean FA, AD, and RD of each region using the same method as for whole CC analysis, comparing both groups using unpaired two sample *t*-tests. For this analysis, *t*-tests were performed 15 times (five ROI × three parameters), so after Bonferroni correction, the statistical threshold was set at $P < 0.0033$ (= 0.05/15).

Functional analysis of *NgR1* 3' enhancer

Epigenomics data

ChIP-seq and DNaseI-seq data were obtained from the ENCODE Project (http://genome.ucsc.edu/ENCODE). ENCODE Project data were displayed in the University of California, Santa Cruz (UCSC) Genome Browser (http://genome.ucsc.edu).

Luciferase assays

DNA fragments corresponding to a candidate enhancer region (chr22: 20224442-20228467) and a 5'-deleted region (chr22: 20224442-20227395, 20228125-20228467) were polymerase chain reaction (PCR) amplified from human genomic DNA and cloned into the pGL4.50 plasmid (Promega, Madison, WI, USA) at the BamHI site using the In-Fusion HD cloning kit (Takara, Otsu, Japan) to generate reference-CMV, rs701428-CMV and reference-S-CMV plasmids. PCR fragments were Sanger sequenced in both directions to confirm presence of the rs701428 SNP and absence of PCR amplification-induced mutations.

Reporter plasmids were co-transfected into mouse cortical neurons with constitutively active pRL-CMV *Renilla* luciferase (Promega) as the control plasmid, using a NEPA21 electroporator (Nepagene, Chiba, Japan). C57BL/6 mouse E16.5 embryo cortices were dissected and dissociated using a neural tissue dissociation kit (P) (Miltenyi-Biotec, Bergisch Gladbach, Germany). To fully dissociate cells, trituration was performed using a flame-narrowed Pasteur pipette. Dissociated mouse cortical neurons were centrifuged at 90 ×g for 5 min at 4°C and resuspended in a 100 µl mixture of Opti-MEM (Invitrogen, Carlsbad, CA, USA) and reporter plasmid. Two types of electric pulse were applied (poring pulse condition: 275 V; pulse length, 0.5 ms; two pulses; interval between pulses, 50 ms; decay, 10%; rate with + polarity. Transfer pulse condition: 20 V; pulse length, 50 ms; five pulses; interval between the pulses, 50 ms; decay, 40%; rate with +/- polarity). After electroporation, cells were immediately seeded onto polyornithine-coated 96-well plates (Nunc, Naperville, IL, USA). Plates were precoated overnight with polyornithine (30 mg/ml; Sigma, St Louis, MO, USA) in water, and washed three times with water before use. Neurons were maintained in Neurobasal Medium containing B27 supplement (2%; Invitrogen), penicillin-streptomycin (100

mg/ml penicillin, 100 U/ml streptomycin; Nacalai Tesque) and glutamine (2 mM; Life Technologies, Gaithersburg, MD, USA), and grown *in vitro* for 6 days. One half of the medium was replaced with fresh warm medium on the 2nd, 4th and 6th days *in vitro* (DIV). DIV 6 neurons were incubated for 12 hours in 1 μM tetrodotoxin (Tocris, Bristol, UK) and 100 μM D(-)-2-amino-5-phosphonopentanoic acid (Tocris), and then for 6 hours in 55 mM KCl. Next, cells were harvested and extracts assayed for luciferase activity using the Dual-Luciferase Reporter Assay System (Promega), with measurements performed using a Varioskan (Thermo Fisher Scientific, Waltham, MA, USA). The luminescence ratio of experimental sample to control reporter was calculated for each sample and defined as the relative luciferase unit.

Electrophoretic mobility shift assay (EMSA)

DNA binding reactions were performed in 20 μl reaction volumes containing 50 fmol end-labeled dsDNA probe and 2 μg nuclear extract in Gel Shift assay system buffer (Thermo Fisher Scientific). Reaction mixtures were incubated at room temperature for 30 min, loaded onto 6% native polyacrylamide gels, and run in 0.5 × Tris-boric acid-EDTA buffer at 130 V for 4 hours. For competition experiments, cold probe (10-fold molar excess of unlabeled oligonucleotide) was added, with the probe added last.

Nuclear extracts from control and c-MYB, MYBL1, or MYBL2-transfected 293 cells were prepared using the NE-PER nuclear and cytoplasmic extraction kits (Thermo Fisher Scientific). Upper strand sequences for double-stranded oligonucleotides were: schizophrenia risk rs701428-A allele probe: 5'-CTGAAGGAGAGTTGGGCGGGTCAGG-3'; and reference-G allele probe:

5'-CTGAAGGAGAGTCGGGCGGGTCAGG-3'. Oligonucleotide probes were labeled and subjected to gel shift assay using the biotin 3' end labeling and Light-Shift Chemiluminescent EMSA kits (Thermo Fisher Scientific). To anneal complementary oligonucleotides, sense and antisense oligonucleotides were combined and incubated at 95°C for 5 min. Binding reactions containing 10 × binding buffer, 1 μg poly(dI-dC), 5 mM $MgCl_2$, 2.5 % glycerol, and 6 μg nuclear extract were incubated with biotin-labeled oligonucleotides (20 fmol per oligonucleotide), in the absence or presence of a 200-fold molar excess of unlabeled competitor, for 20 min at room temperature. For competition studies, increasing concentrations of unlabeled oligonucleotides were added to binding reactions. Samples were then run on a native 5% polyacrylamide gel. Gel contents were transferred to nylon membranes (Hybond-N+, GE Healthcare Life Sciences, Piscataway, NJ, USA) and crosslinked to the membrane using a UV crosslinker. Membranes were blocked and visualized using the Light-Shift kit.

Results

Demographic data

Characteristics of the participants are shown in Table 1. No significant difference between G homozygous and A carrier groups was found with regard to age, sex, handedness, education, or IQ.

Whole CC imaging

The A carrier group had significantly larger whole CC volumes, compared with the G homozygous group (Figure 2A), which was also confirmed using a permutation test (empirical P value =0.026). There were no significant differences in whole CC DTI indices (Table 2). We also analyzed the data with age included as a covariate, and the

group difference was reproduced.

CC subregion imaging

The A carrier group showed a trend towards a larger anterior CC volume compared with the G homozygous group, although the difference was non-significant after Bonferroni correction (Table 3). With regard to DTI indices, mean RD in the central CC region was significantly smaller in the A carrier group compared with the G homozygous group (Figure 2B, Table 4).

Functional analysis of the *NgR1* 3′ enhancer

The 3′ region of *NgR1* harbors regulatory elements

Multiple species alignment of the region surrounding the rs701428 SNP was examined in the University of California, Santa Cruz (UCSC) genome browser Multiz alignment track.[31, 32] The *NgR1* 3′ region is highly conserved and is, therefore, likely to contain enhancer elements (Figure 3). Regulatory elements such as active promoters and enhancers are commonly found in open chromatin regions, which can be identified using genome-wide DNase I hypersensitivity assays (DNase I-seq) (ENCODE Consortium) [33-35]. The rs701428 SNP in the *NgR1* 3′ region was mapped within a DNase I hypersensitive site in human prefrontal cortex (Figure 3). To determine if this region harbors enhancers, we examined histone H3 lysine 4 mono-methylation (H3K4me1) and lysine 9 acetylation (H3K9ac), markers of enhancers (ENCODE Consortium).[36-38] H3K4me1 and H3K9ac enrichment suggest that the *NgR1* 3′ region is an active regulatory element (Figure 3).

The presence of overlapping H3K4me1, H3K9ac, and DNase I hypersensitivity peaks suggest the presence of an enhancer in the *NgR1* 3′ region. To investigate if this region

has potential enhancer activity, chr22: 20224442-20228467 was PCR amplified and cloned into a luciferase reporter gene. It has been reported that *NgR1* expression is down-regulated by neuronal activity [39]. To examine the effect of neuronal activity on the putative *NgR1* 3′ enhancer, we transfected 3′ enhancer reporter constructs with or without the rs701428 SNP into primary cortical neurons. Substantial increases in luciferase activity were observed for both constructs in the presence of the sodium channel blocker tetrodotoxin (TTX), and the NMDA receptor antagonist, D(-)-2-amino-5-phosphonopentanoic acid (D-AP5), which blocks neuronal activity (Figure 4B). Conversely, neuronal depolarization by elevated potassium chloride (KCl) levels drastically decreased transactivation activity of the *NgR1* 3′ region.

The rs701428 SNP may alter transcription factor recruitment to the *NgR1* 3′ enhancer. We used JASPAR [40] to screen for potential transcription factor binding sites in the region surrounding rs701428, and found binding affinity for the myeloblastosis (MYB) family for the schizophrenia risk rs701428-A allele but not for the reference G allele (Figure 4C). The MYB family contains three members (c-MYB, MYBL1, and MYBL2), which bind DNA with similar specificity [41, 42]. MYBL2 over-expression specifically decreased transactivation activity of the 3′ *NgR1* enhancer with the schizophrenia risk rs701428-A allele (Figure 4D). In contrast, neither the 3′ *NgR1* enhancer containing the reference rs701428-G allele nor with a deletion of a 5′ 700 bp region containing rs701428 was affected by MYBL2 over-expression (Figure 4E and F). To examine if the MYB transcription factor family binds to the region with the schizophrenia risk rs701428-A allele, we performed EMSA. The labeled schizophrenia risk rs701428-A allele probe, but not the labeled reference-G allele probe, formed a binding complex with c-MYB, MYBL1, and MYBL2 (Figure 5A, arrow). Furthermore, MYBL2 binding

to the labeled rs701428-A allele probe was diminished in the presence of a 200-fold excess of unlabeled rs701428-A allele probe but not unlabeled reference-G allele probe (Figure 5B, arrow).

Discussion

In the present study, the rs701428 polymorphism located in the 3′ region of the *NgR1* gene, was found to be associated with CC structural variation in the human brain. Minor A allele carriers of this SNP, which was reported as the risk allele for schizophrenia in a previous study [26], had larger whole CC volumes and lower RD in the central CC region, compared with major G allele homozygous participants. Furthermore, we demonstrated that the *NgR1* 3′ region containing rs701428 is a neuronal-activity-dependent enhancer, and that the schizophrenia risk allele A of rs701428 renders this enhancer susceptible to transcriptional regulation by MYBL2.

In 22q11.2DS, structural brain abnormalities that are likely to be developmental in nature have been repeatedly reported.[14, 20, 22] However, how and which genetic changes in this chromosomal region induce morphological brain abnormalities are not known. Our study is the first to implicate a specific gene as a candidate for the morphological changes to the brain in this syndrome, as well as a possible mechanism. As the genetic polymorphism investigated in our study is associated with schizophrenia [26, 27], the putative molecular mechanism identified may, in part, be involved in the neurodevelopmental manifestation of schizophrenia pathology.

NgR1, a receptor for Nogo-A, represses synaptogenesis and axonal sprouting [43] and is down-regulated by neuronal activity [39, 44, 45]. This NgR1-mediated mechanism is thought to be important for restricting synaptic plasticity and maintaining preformed

neuronal wiring [5, 39]. We show that the 3′ region of the *NgR1* gene, containing rs701428, is a neuronal-activity-dependent enhancer, and that the minor (schizophrenia risk) allele of rs701428 disinhibits repressive activity of this enhancer via MYBL2 binding. These results suggest that the risk allele may dysregulate *NgR1* expression, and consequently disturb the regulatory process of restricting synaptic plasticity, a requirement for normal neural circuitry development.

Our MRI analyses found that minor (schizophrenia risk) allele carriers have larger CC volumes. This finding is compatible with previous MRI studies reporting enlarged CC volumes in 22q11.2DS patients [18]. CC enlargement in rs701428 minor allele carriers may be reasonably expected, considering the putative role of *NgR1* in neural circuitry formation [46]. *NgR1* suppresses excessive branching of axon fibers [5]. The expression of *NgR1* is downregulated by neuronal activation [39]. This mechanism plays pivotal roles in the neuronal activity-dependent regulation of axonal structures. Dysregulated NgR expression in minor allele carriers may disrupt normal synaptic pruning, and may result in abnormal hypertrophic white matter tracts. As the CC is the largest white matter tract in the human brain, our MRI data, as well as previous MRI studies on 22q11.2DS, may have captured a more general process of white matter wiring abnormalities.

In schizophrenia, structural MRI studies are not unanimous with regard to the structural abnormalities of the CC. Both increased and decreased CC volumes in schizophrenia patients have been previously documented [47]. The white matter alteration in schizophrenia might be caused by the interaction between genetic variation within the 22q11.2 region and variation in other risk genes for schizophrenia, such as neureglin 1 (*NRG1*), *ERBB4* and disrupted-in-schizophrenia 1 (*DISC1*). Dysfunction of these genes

has been reported to alter myelination, similarly to *NgR1* [48-50]. In humans, variation of *ERBB4* was demonstrated to associate with subcortical microstructure [51]. Therefore, the differential contribution of these multiple genes among individuals may result in the white matter structural variations of schizophrenia, reflecting heterogeneity of the disease. Our data show that the putative neurodevelopmental molecular mechanism mediated by *NgR1* may partially explain the white matter pathology of schizophrenia.

Furthermore, this *NgR1* mechanism may also show regional specificity in addition to a process involving axonal development and synapse formation at the whole brain level. Indeed, our data show that minor allele carriers have decreased RD in the central region of the CC. DTI studies on 22q11.2DS are in agreement with this finding, showing a genetic effect localized in specific CC regions [21, 22]. Our result, however, is inconsistent with that of Perlstein et al [28], who investigated the effect of the same SNP, rs701428, and reported that the G allele is associated with reduced RD [28]. The discrepancy might be due to the difference of the white matter regions reported to be associated with the allelic variation. In addition, it should be noted that Perlstein et al. investigated this association in 22q11.2 deletion syndrome individuals; a variation of *NgR1* might have complex genetic interaction with other genes in the deleted 22q11.2 region, which are important for neuronal differentiation and function [11, 52].

A major limitation of our study is the relatively small sample size. Another is that we focused on CC structure and not on the other brain abnormalities reported in 22q11.2DS. Our present results are highly preliminary until replicated with larger sample numbers.

In summary, our study shows that *NgR1* can influence macro- and micro- white matter structure of the human brain. A frequently reported structural anomaly in 22q11.2DS,

namely CC enlargement, can be partially affected by disrupted regulation of *NgR1*. Furthermore, a 22q11 model mouse study is expected to reveal the possible contribution of *NgR1* to CC structural variation.

Acknowledgements

The authors wish to extend their gratitude to Dr Sin-ichi Urayama for his assistance in data acquisition and processing, and most of all, to the volunteers for participating in the study. This work was in part funded by Takeda Pharmaceutical Company Limited.

Conflict of Interest

The authors declare no conflict of interest.

References

1. GrandPre T, Li S, Strittmatter SM. Nogo-66 receptor antagonist peptide promotes axonal regeneration. Nature 2002; 417(6888): 547-551.

2. McGee AW, Strittmatter SM. The Nogo-66 receptor: focusing myelin inhibition of axon regeneration. Trends Neurosci 2003; 26(4): 193-198.

3. Li S, Kim JE, Budel S, Hampton TG, Strittmatter SM. Transgenic inhibition of Nogo-66 receptor function allows axonal sprouting and improved locomotion after spinal injury. Mol Cell Neurosci 2005; 29(1): 26-39.

4. Fournier AE GT, Strittmatter SM Identifcation of a receptor mediating Nogo-66 inhibition of axonal regeneration. Nature 2001; 409: 6.

5. Zagrebelsky M, Schweigreiter R, Bandtlow CE, Schwab ME, Korte M. Nogo-A stabilizes the architecture of hippocampal neurons. J Neurosci 2010; 30(40): 13220-13234.

6. Akbik FV, Bhagat SM, Patel PR, Cafferty WB, Strittmatter SM. Anatomical plasticity of adult brain is titrated by Nogo Receptor 1. Neuron 2013; 77(5): 859-866.

7. Hunt D. Nogo Receptor mRNA Expression in Intact and Regenerating CNS Neurons. Mol Cell Neurosci 2002; 20(4): 537-552.

8. Josephson A, Trifunovski A, Widmer HR, Widenfalk J, Olson L, Spenger C. Nogo-receptor gene activity: cellular localization and developmental regulation of mRNA in mice and humans. J Comp Neurol 2002; 453(3): 292-304.

9. Shaikh TH, Kurahashi H, Saitta SC, O'Hare AM, Hu P, Roe BA, Driscoll DA, McDonald-McGinn DM, Zackai EH, Budarf ML, Emanuel BS. Chromosome 22-specific low copy repeats and the 22q11.2 deletion syndrome: genomic organization and deletion endpoint analysis. Hum Mol Genet 2000; 9(4): 489-501.

10. Pulver AE, Nestadt G, Goldberg R, Shprintzen RJ, Lamacz M, Wolyniec PS, Morrow B, Karayiorgou M, Antonarakis SE, Housman D, Kucherlapati R. Psychotic Illness in Patients Diagnosed with Velo-Cardio-Facial Syndrome and Their Relatives. J Nerv Ment Dis 1994; 182(8): 476-478.

11. Toritsuka M, Kimoto S, Muraki K, Landek-Salgado MA, Yoshida A, Yamamoto N, Horiuchi Y, Hiyama H, Tajinda K, Keni N, Illingworth E, Iwamoto T, Kishimoto T, Sawa A, Tanigaki K. Deficits in microRNA-mediated Cxcr4/Cxcl12 signaling in neurodevelopmental deficits in a 22q11 deletion syndrome mouse model. Proc Natl Acad Sci U S A 2013; 110(43): 17552-17557.

12. Drew LJ, Crabtree GW, Markx S, Stark KL, Chaverneff F, Xu B, Mukai J, Fenelon K, Hsu PK, Gogos JA, Karayiorgou M. The 22q11.2 microdeletion: fifteen years of insights into the genetic and neural complexity of psychiatric disorders. Int J Dev Neurosci 2011; 29(3): 259-281.

13. Chow EW, Mikulis DJ, Zipursky RB, Scutt LE, Weksberg R, Bassett AS. Qualitative MRI findings in adults with 22q11 deletion syndrome and schizophrenia. Biol Psychiatry 1999; 46(10): 1436-1442.

14. Amelsvoort TV. Structural brain abnormalities associated with deletion at chromosome 22q11: Quantitative neuroimaging study of adults with velo-cardio-facial syndrome. Br J Psychiatry 2001; 178(5): 412-419.

15. Sztriha L, Guerrini R, Harding B, Stewart F, Chelloug N, Johansen JG. Clinical, MRI, and pathological features of polymicrogyria in chromosome 22q11 deletion syndrome. Am J Med Genet A 2004; 127A(3): 313-317.

16. Eliez S, Schmitt JE, White CD, Reiss AL. Children and adolescents with velocardiofacial syndrome: a volumetric MRI study. Am J Psychiatry 2000; 157(3): 409-415.

17. Debbane M, Schaer M, Farhoumand R, Glaser B, Eliez S. Hippocampal volume reduction in 22q11.2 deletion syndrome. Neuropsychologia 2006; 44(12): 2360-2365.

18. Ryan AK, Goodship JA, Wilson DI, Philip N, Levy A, Seidel H, Schuffenhauer S, Oechsler H, Belohradsky B, Prieur M, Aurias A, Raymond FL, Clayton-Smith J, Hatchwell E, McKeown C, Beemer FA, Dallapiccola B, Novelli G, Hurst JA, Ignatius J, Green AJ, Winter RM, Brueton L, Brondum-Nielsen K, Scambler PJ, et al. Spectrum of clinical features associated with interstitial chromosome 22q11 deletions: a European collaborative study. J Med Genet 1997; 34(10): 798-804.

19. Machado AM, Simon TJ, Nguyen V, McDonald-McGinn DM, Zackai EH, Gee JC. Corpus callosum morphology and ventricular size in chromosome 22q11.2 deletion syndrome. Brain Res 2007; 1131(1): 197-210.

20. Tan GM, Arnone D, McIntosh AM, Ebmeier KP. Meta-analysis of magnetic resonance imaging studies in chromosome 22q11.2 deletion syndrome (velocardiofacial syndrome). Schizophr Res 2009; 115(2-3): 173-181.

21. Simon TJ, Ding L, Bish JP, McDonald-McGinn DM, Zackai EH, Gee J. Volumetric, connective, and morphologic changes in the brains of children with chromosome 22q11.2 deletion syndrome: an integrative study. NeuroImage 2005; 25(1): 169-180.

22. Barnea-Goraly N, Menon V, Krasnow B, Ko A, Reiss A, Eliez S. Investigation of white matter structure in velocardiofacial syndrome: a diffusion tensor imaging study. Am J Psychiatry 2003; 160(10): 1863-1869.

23. Arnone D, McIntosh AM, Tan GM, Ebmeier KP. Meta-analysis of magnetic resonance imaging studies of the corpus callosum in schizophrenia. Schizophr Res 2008; 101(1-3): 124-132.

24. David AS. Schizophrenia and the corpus callosum: developmental, structural and functional relationships. Behav Brain Res 1994; 64(1-2): 203-211.

25. da Silva Alves F, Schmitz N, Bloemen O, van der Meer J, Meijer J, Boot E, Nederveen A, de Haan L, Linszen D, van Amelsvoort T. White matter abnormalities in adults with 22q11 deletion syndrome with and without schizophrenia. Schizophr Res 2011; 132(1): 75-83.

26. Budel S, Padukkavidana T, Liu BP, Feng Z, Hu F, Johnson S, Lauren J, Park JH, McGee AW, Liao J, Stillman A, Kim JE, Yang BZ, Sodi S, Gelernter J, Zhao H, Hisama F, Arnsten AF, Strittmatter SM. Genetic variants of Nogo-66 receptor with possible association to schizophrenia block myelin inhibition of axon growth. J Neurosci 2008; 28(49): 13161-13172.

27. Liu H, Abecasis GR, Heath SC, Knowles A, Demars S, Chen YJ, Roos JL, Rapoport JL, Gogos JA, Karayiorgou M. Genetic variation in the 22q11 locus and susceptibility to schizophrenia. Proc Natl Acad Sci U S A 2002; 99(26): 16859-16864.

28. Perlstein MD, Chohan MR, Coman IL, Antshel KM, Fremont WP, Gnirke MH, Kikinis Z, Middleton FA, Radoeva PD, Shenton ME, Kates WR. White matter abnormalities in 22q11.2 deletion syndrome: preliminary associations with the Nogo-66 receptor gene and symptoms of psychosis. Schizophr Res 2014; 152(1): 117-123.

29. Desikan RS, Segonne F, Fischl B, Quinn BT, Dickerson BC, Blacker D, Buckner RL, Dale AM, Maguire RP, Hyman BT, Albert MS, Killiany RJ. An automated labeling system for subdividing the human cerebral cortex on MRI scans into gyral based regions of interest. NeuroImage 2006; 31(3): 968-980.

30. Buckner RL, Head D, Parker J, Fotenos AF, Marcus D, Morris JC, Snyder AZ. A unified approach for morphometric and functional data analysis in young, old, and demented adults using automated atlas-based head size normalization: reliability and validation against manual measurement of total intracranial volume. NeuroImage 2004; 23(2): 724-738.

31. Karolchik D, Barber GP, Casper J, Clawson H, Cline MS, Diekhans M, Dreszer TR, Fujita PA, Guruvadoo L, Haeussler M, Harte RA, Heitner S, Hinrichs AS, Learned K, Lee BT, Li CH, Raney BJ, Rhead B, Rosenbloom KR, Sloan CA, Speir ML, Zweig AS, Haussler D, Kuhn RM, Kent WJ. The UCSC Genome Browser database: 2014 update. Nucleic Acids Res 2014; 42(Database issue): D764-770.

32. Blanchette M, Kent WJ, Riemer C, Elnitski L, Smit AF, Roskin KM, Baertsch R, Rosenbloom K, Clawson H, Green ED, Haussler D, Miller W. Aligning multiple genomic sequences with the threaded blockset aligner. Genome Res 2004; 14(4): 708-715.

33. Hesselberth JR, Chen X, Zhang Z, Sabo PJ, Sandstrom R, Reynolds AP, Thurman RE, Neph S, Kuehn MS, Noble WS, Fields S, Stamatoyannopoulos JA. Global mapping of protein-DNA interactions in vivo by digital genomic footprinting. Nat Methods 2009; 6(4): 283-289.

34. Boyle AP, Song L, Lee BK, London D, Keefe D, Birney E, Iyer VR, Crawford GE, Furey TS. High-resolution genome-wide in vivo footprinting of diverse transcription factors in human cells. Genome Res 2011; 21(3): 456-464.

35. Pique-Regi R, Degner JF, Pai AA, Gaffney DJ, Gilad Y, Pritchard JK. Accurate inference of transcription factor binding from DNA sequence and chromatin accessibility data. Genome Res 2011; 21(3): 447-455.

36. Heintzman ND, Stuart RK, Hon G, Fu Y, Ching CW, Hawkins RD, Barrera LO, Van Calcar S, Qu C, Ching KA, Wang W, Weng Z, Green RD, Crawford GE, Ren B. Distinct and predictive chromatin signatures of transcriptional promoters and enhancers in the human genome. Nat Genet 2007; 39(3): 311-318.

37. Heintzman ND, Hon GC, Hawkins RD, Kheradpour P, Stark A, Harp LF, Ye Z, Lee LK, Stuart RK, Ching CW, Ching KA, Antosiewicz-Bourget JE, Liu H, Zhang X, Green RD, Lobanenkov VV, Stewart R, Thomson JA, Crawford GE, Kellis M, Ren B. Histone modifications at human enhancers reflect global cell-type-specific gene expression. Nature 2009; 459(7243): 108-112.

38. Lupien M, Eeckhoute J, Meyer CA, Wang Q, Zhang Y, Li W, Carroll JS, Liu XS, Brown M. FoxA1 translates epigenetic signatures into enhancer-driven lineage-specific transcription. Cell 2008; 132(6): 958-970.

39. Wills ZP, Mandel-Brehm C, Mardinly AR, McCord AE, Giger RJ, Greenberg ME. The nogo receptor family restricts synapse number in the developing hippocampus. Neuron 2012; 73(3): 466-481.

40. Mathelier A, Zhao X, Zhang AW, Parcy F, Worsley-Hunt R, Arenillas DJ, Buchman S, Chen CY, Chou A, Ienasescu H, Lim J, Shyr C, Tan G, Zhou M, Lenhard B, Sandelin A, Wasserman WW. JASPAR 2014: an extensively expanded and updated open-access database of transcription factor binding profiles. Nucleic Acids Res 2014; 42(Database issue): D142-147.

41. Howe KM, Watson RJ. Nucleotide preferences in sequence-specific recognition of DNA by c-myb protein. Nucleic Acids Res 1991; 19(14): 3913-3919.

42. Golay J, Loffarelli L, Luppi M, Castellano M, Introna M. The human A-myb protein is a strong activator of transcription. Oncogene 1994; 9(9): 2469-2479.

43. Craveiro LM, Hakkoum D, Weinmann O, Montani L, Stoppini L, Schwab ME. Neutralization of the membrane protein Nogo-A enhances growth and reactive sprouting in established organotypic hippocampal slice cultures. Eur J Neurosci 2008; 28(9): 1808-1824.

44. Lee H, Raiker SJ, Venkatesh K, Geary R, Robak LA, Zhang Y, Yeh HH, Shrager P, Giger RJ. Synaptic function for the Nogo-66 receptor

NgR1: regulation of dendritic spine morphology and activity-dependent synaptic strength. J Neurosci 2008; 28(11): 2753-2765.

45. Borrie SC, Baeumer BE, Bandtlow CE. The Nogo-66 receptor family in the intact and diseased CNS. Cell Tissue Res 2012; 349(1): 105-117.

46. Whitford TJ, Savadjiev P, Kubicki M, O'Donnell LJ, Terry DP, Bouix S, Westin CF, Schneiderman JS, Bobrow L, Rausch AC, Niznikiewicz M, Nestor PG, Pantelis C, Wood SJ, McCarley RW, Shenton ME. Fiber geometry in the corpus callosum in schizophrenia: evidence for transcallosal misconnection. Schizophr Res 2011; 132(1): 69-74.

47. Shenton ME, Dickey CC, Frumin M, McCarley RW. A review of MRI findings in schizophrenia. Schizophr Res 2001; 49(1-2): 1-52.

48. Michailov GV, Sereda MW, Brinkmann BG, Fischer TM, Haug B, Birchmeier C, Role L, Lai C, Schwab MH, Nave KA. Axonal neuregulin-1 regulates myelin sheath thickness. Science 2004; 304(5671): 700-703.

49. Roy K, Murtie JC, El-Khodor BF, Edgar N, Sardi SP, Hooks BM, Benoit-Marand M, Chen C, Moore H, O'Donnell P, Brunner D, Corfas G. Loss of erbB signaling in oligodendrocytes alters myelin and dopaminergic function, a potential mechanism for neuropsychiatric disorders. Proc Natl Acad Sci U S A 2007; 104(19): 8131-8136.

50. Wood JD, Bonath F, Kumar S, Ross CA, Cunliffe VT. Disrupted-in-schizophrenia 1 and neuregulin 1 are required for the specification of oligodendrocytes and neurones in the zebrafish brain. Hum Mol Genet 2009; 18(3): 391-404.

51. Konrad A, Vucurevic G, Musso F, Stoeter P, Dahmen N, Winterer G. ErbB4 genotype predicts left frontotemporal structural connectivity in human brain. Neuropsychopharmacology 2009; 34(3): 641-650.

52. Kimoto S, Muraki K, Toritsuka M, Mugikura S, Kajiwara K, Kishimoto T, Illingworth E, Tanigaki K. Selective overexpression of Comt in prefrontal cortex rescues schizophrenia-like phenotypes in a mouse model of 22q11 deletion syndrome. Transl Psychiatry 2012; 2: e146.

Figure Legends

Figure 1

Segmented CC is shown. (A) CC labels derived from a FreeSurfer template image. (B) Rigid-body transformed image of segmented CC ROI from MNI302 to MNI152 space.

Figure 2

(A) Scatter plot of whole CC volume versus genotype. Genotype segregates with CC volume.

(B) Scatter plot of RD in the central region of the CC versus genotype.

Figure 3. Epigenetic annotation of the *NgR1* gene

The UCSC Genome Browser screen shot showing the ~50 Kb region surrounding the rs701428 SNP in the *NgR1* gene 3′ region. The lower panel represents an enlarged view of the rs701428 SNP. H3K4me1 and H3K9ac enrichment from NT2-D1 cells, DNaseI-seq enrichment from human prefrontal cortex, and multi-percent identity plot alignment of genomic sequences from eight species are indicated.

Figure 4. The region surrounding rs701428 acts as a neuronal activity-dependent enhancer modulated by Mybl2.

(A) Schematic representation of *NgR1* 3′ enhancer reporter constructs.

(B-F) The *NgR1* 3′ enhancer is downregulated by neuronal activation induced by KCl, and enhanced by blockade of neuronal activation by TTX and D-AP5 (B). Representative Myb binding motif is shown within rs701428 (C). Alleles of rs701428 are shown: the reference G allele (green) and variant A allele (red). Mybl2

overexpression decreases transcriptional repression by neuronal activity of the *NgR1* 3′ enhancer with the schizophrenia risk rs701428-A allele (D), but not the reference-G allele (E), or with deletion of a region containing rs701428 (F). Data are presented as mean ± SD, with each experiment conducted in triplicate.

Figure 5. DNA fragments containing the rs701428 schizophrenia risk A allele but not the reference G allele show specific binding to Myb family transcription factors.

(A) Myb family transcription factor binding was examined using EMSA.

293T cells were transfected with vectors containing c-Myb, Mybl1, Mybl2, or no insert (negative control (NC)). Nuclear extracts were prepared and EMSA performed using reference G allele or schizophrenia risk A allele probes. A background band due to endogenous factors expressed in 293T cells is observed with the rs701428-A allele probe.

(B) Specific binding of Mybl2 to the rs701428-A allele probe but not to the reference G allele probe.

Mybl2-transfected nuclear extracts were incubated with labeled rs701428-A or -G allele probes. Binding was competed using a 200-fold molar excess of unlabeled A or G allele competitor.

Headings of Tables

Table 1

Demographic characteristics of the two groups

Table 2

Group differences of diffusivity parameters (FA, AD, and RD) in whole CC

Table 3

Group differences of volumes in separated CC ROI

Table 4

Group differences of DTI indices (FA, AD, and RD) in separated CC ROI

Figures and Tables

Figure 1

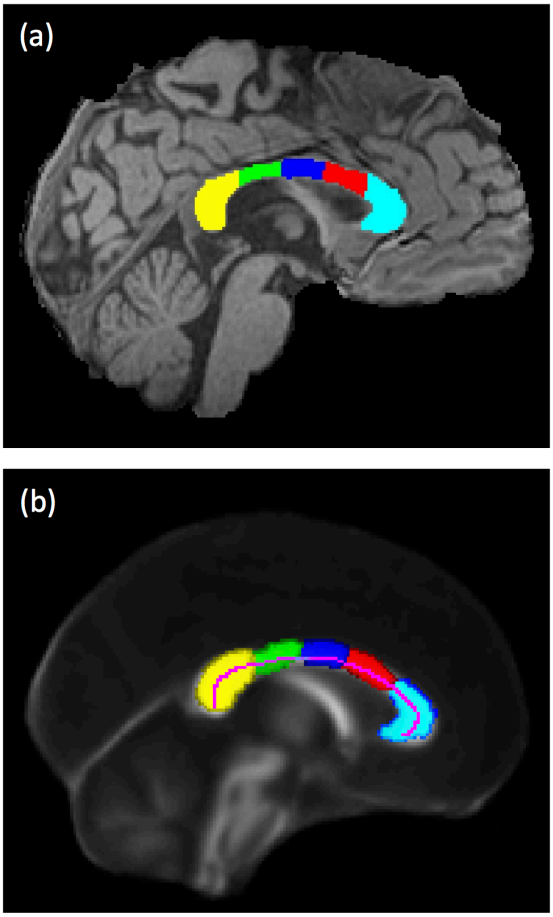

Figure 2

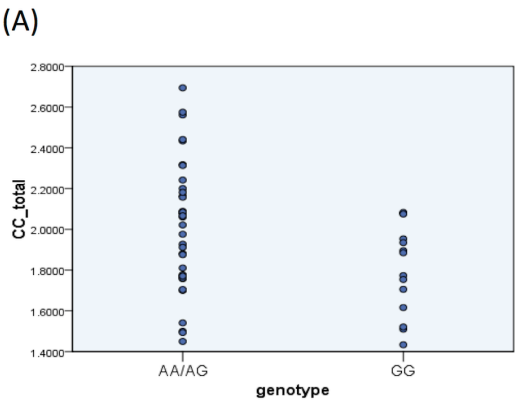

	Genotype		P Value
	AA/AG	GG	
CC Volume	2.010	1.801	0.028*

*p<0.05 (2 sample t test)

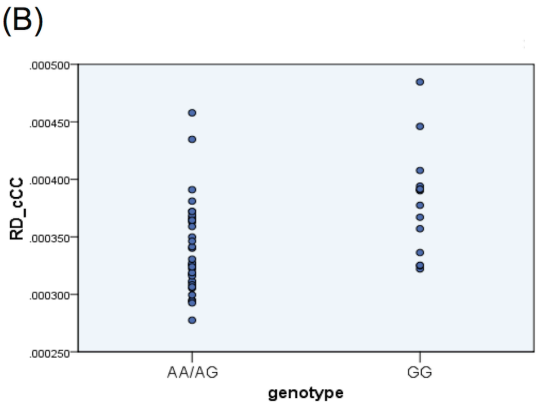

	Genotype		P Value
	AA/AG	GG	
RD of CC	$3.800*10^{-5}$	$4.257*10^{-5}$	0.003**

**p<0.0033(2 sample t test)

Figure 3

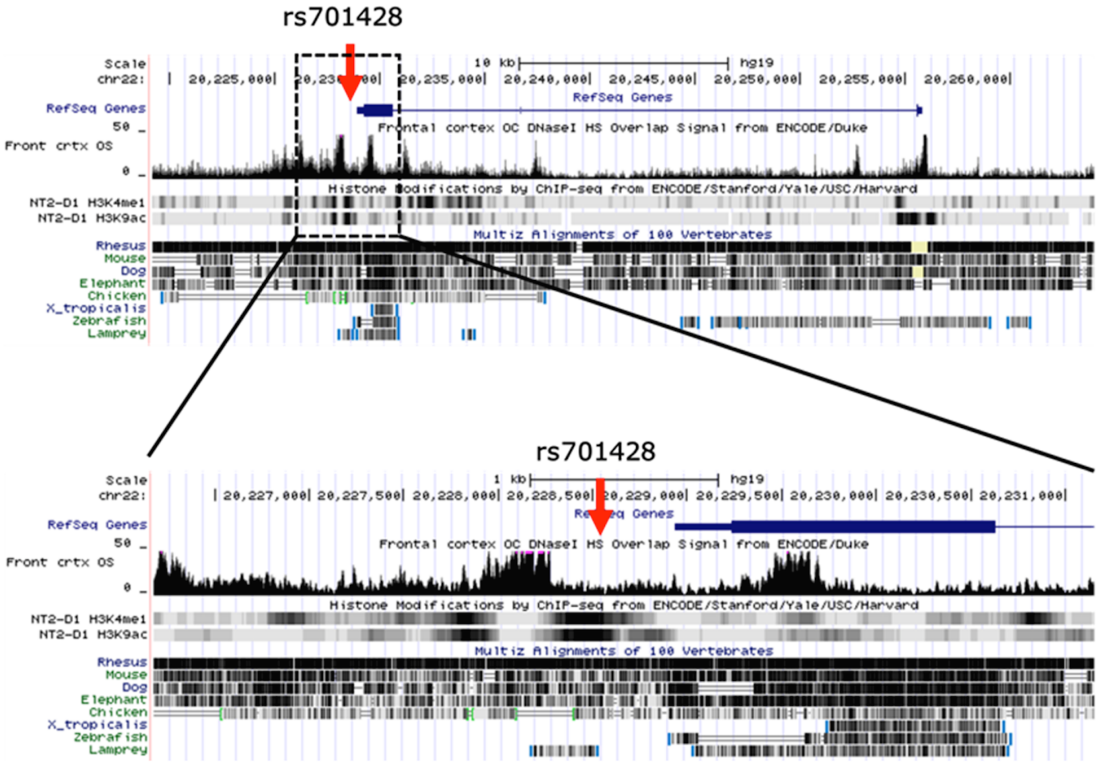
rs701428
Scale
chr22:
10 kb
hg19
20,225,000
20,235,000
20,240,000
20,245,000
20,250,000
20,255,000
20,260,000
RefSeq Genes
Frontal cortex OC DNaseI HS Overlap Signal from ENCODE/Duke
Front crtx OS
50
0
Histone Modifications by ChIP-seq from ENCODE/Stanford/Yale/USC/Harvard
NT2-D1 H3K4me1
NT2-D1 H3K9ac
Multiz Alignments of 100 Vertebrates
Rhesus
Mouse
Dog
Elephant
Chicken
X_tropicalis
Zebrafish
Lamprey
rs701428
1 kb
hg19
20,227,000
20,227,500
20,228,000
20,228,500
20,229,000
20,229,500
20,230,000
20,230,500
20,231,000
RefSeq Genes
Frontal cortex OC DNaseI HS Overlap Signal from ENCODE/Duke
Front crtx OS
50
0
Histone Modifications by ChIP-seq from ENCODE/Stanford/Yale/USC/Harvard
NT2-D1 H3K4me1
NT2-D1 H3K9ac
Multiz Alignments of 100 Vertebrates
Rhesus
Mouse
Dog
Elephant
Chicken
X_tropicalis
Zebrafish
Lamprey

Figure 4

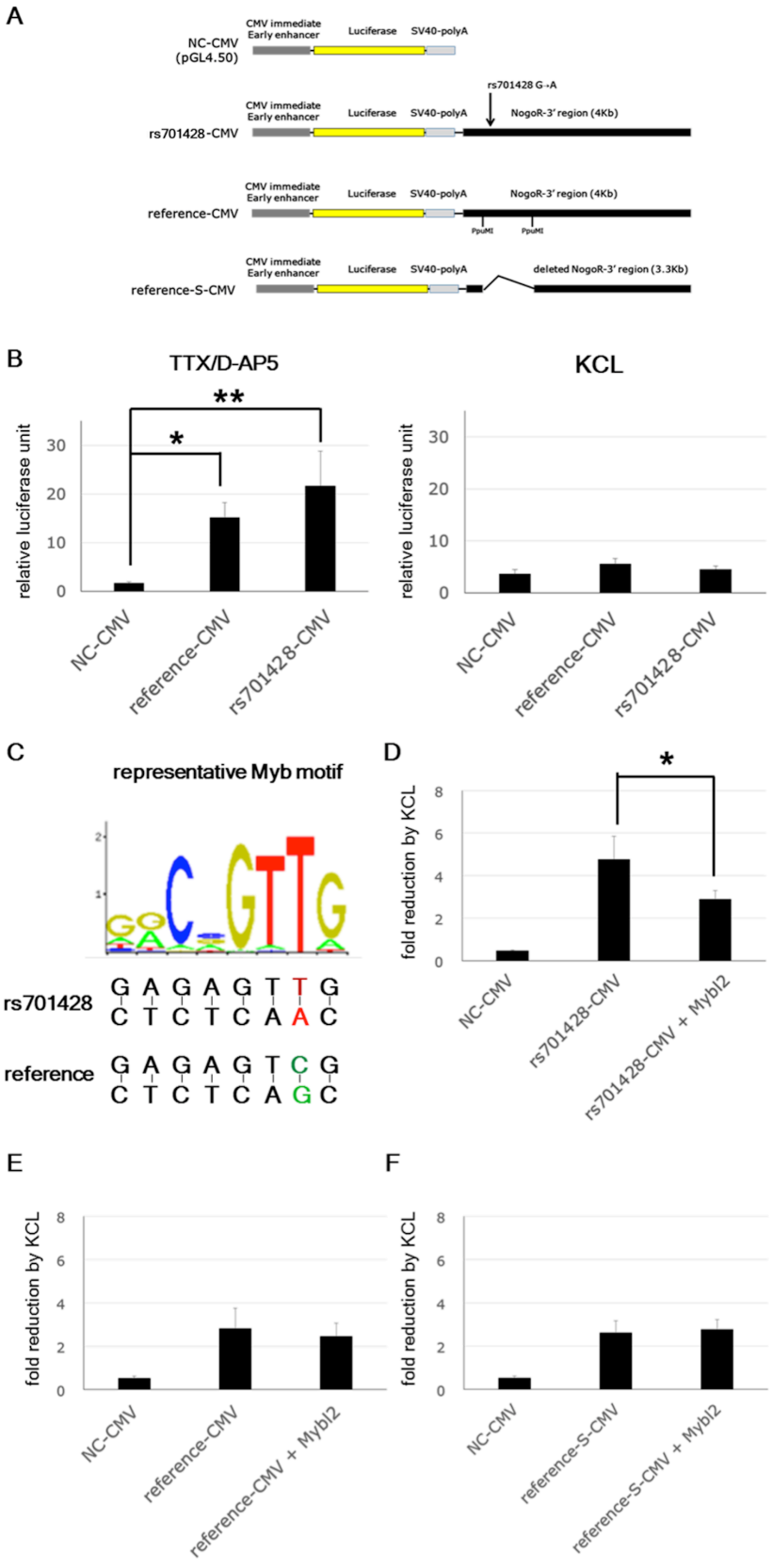
A
NC-CMV (pGL4.50)
CMV immediate Early enhancer
Luciferase
SV40-polyA
rs701428-CMV
rs701428 G→A
NogoR-3′ region (4Kb)
reference-CMV
PpuMI
reference-S-CMV
deleted NogoR-3′ region (3.3Kb)
B
TTX/D-AP5
KCL
relative luciferase unit
NC-CMV
reference-CMV
rs701428-CMV
C
representative Myb motif
rs701428
reference
D
fold reduction by KCL
rs701428-CMV + MybI2
E
reference-CMV + MybI2
F
reference-S-CMV
reference-S-CMV + MybI2

Figure 5

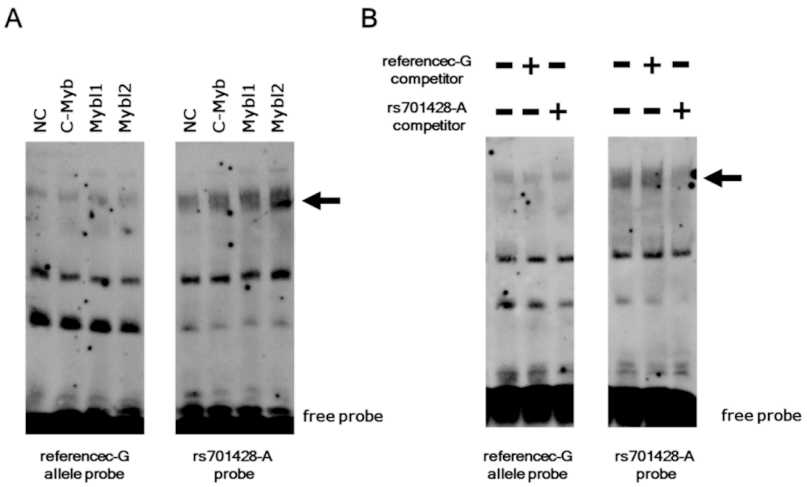

Table 1

	Genotype		Statistic Value (T or χ^2 Value)	P Value
	AA/AG	GG		
Number	36	14	-	-
Age	25.7±6.6	24.1±5.3	0.84	0.41*
Gender (F/M)	16/20	3/11	1.62	0.14**
Education	14.0±2.9	14.3±2.8	0.28	0.78*
VIQ	110.8±17.0	118.9±18.0	1.48	0.15*
PIQ	115.4±17.1	122.5±13.1	1.39	0.17*

*2 sample t test
**Chai square test

Table 2

		Genotype		Degree of Freedom	T Value	P Value*
		AA/AG	GG			
Volume		2.01	1.80	48	1.96	0.028**
Diffusivity	FA	0.682	0.667	48	1.30	0.200
	AD	$1.25*10^{-3}$	$1.26*10^{-3}$	48	0.64	0.525
	RD	$3.47*10^{-4}$	$3.65*10^{-4}$	48	1.39	0.172

*2 sample t test
**p<0.05

Table 3

Region	Genotype		Degree of Freedom	T Value	P Value
	AA/AG	GG			
Whole	2.01	1.80	48	1.96	0.028*
Anterior	0.534	0.467	48	2.06	0.022**
Mid-anterior	0.317	0.281	48	1.17	0.124**
Central	0.313	0.279	48	1.07	0.145**
Mid-posterior	0.280	0.262	48	0.42	0.337**
Posterior	0.566	0.513	48	1.58	0.060**

*2 sample t test

**2 sample t test, corrected by the Bonferroni method

Table 4

Region	Diffusivity	Genotype		T Value	P Value*
		AA/AG	GG		
Anterior	FA	0.678076	0.6800	0.11	0.913
	AD	$1.146*10^{-3}$	$1.134*10^{-3}$	0.35	0.728
	RD	$3.230*10^{-4}$	$3.148*10^{-4}$	0.36	0.722
Mid-anterior	FA	0.635122	0.608152	1.54	0.130
	AD	$1.211*10^{-3}$	$1.240*10^{-3}$	1.09	0.282
	RD	$3.790*10^{-4}$	$4.152*10^{-4}$	1.79	0.079
Central	FA	0.697747	0.668065	2.30	0.026
	AD	$1.310*10^{-3}$	$1.337*10^{-3}$	1.12	0.245
	RD	$3.389*10^{-4}$	$3.797*10^{-4}$	3.14	0.003**
Mid-posterior	FA	0.614926	0.601437	0.71	0.481
	AD	$1.435*10^{-3}$	$1.432*10^{-3}$	0.10	0.919
	RD	$4.894*10^{-4}$	$4.994*10^{-4}$	0.37	0.712
Posterior	FA	0.745049	0.727123	1.33	0.190
	AD	$1.270*10^{-3}$	$1.297*10^{-3}$	1.01	0.317
	RD	$2.837*10^{-4}$	$3.090*10^{-4}$	1.63	0.110

*2 sample t test, corrected by the Bonferroni method

**p<0.0033 (=0.05/15)